Ru(II)-peptide bioconjugates with the cppH linker (cppH = 2-(2'-pyridyl)pyrimidine-4-carboxylic acid): Synthesis, structural characterization, and different stereochemical features between organic and aqueous solvents.

Federica Battistin,[a] Daniel Siegmund,[b] Gabriele Balducci,[a] Enzo Alessio,[a]* Nils Metzler-Nolte[b]*

a) Department of Chemical and Pharmaceutical Sciences, University of Trieste, Via Giorgieri 1, 34127 Trieste, Italy.
Email: alessi@units.it; WWW: http://dscf.units.it/en

b) Ruhr University Bochum, Faculty of Chemistry and Biochemistry, Inorganic Chemistry I – Bioinorganic Chemistry, Bochum, Germany.
Email: nils.metzler-nolte@rub.de; WWW: www.chemie.rub.de/ac1

Supplementary Information

Figures S1-S9. NMR characterization of *trans,cis*-$RuCl_2(CO)_2$(cppH-RRPYIL) (**7**) in DMSO-d_6 and D_2O.
Figures S10-S13. NMR characterization of [Ru([9]aneS_3)(cppH-RRPYIL)(PTA)]$^{2+}$ (**8**) in DMSO-d_6 and D_2O.
Figures S14-S15. NMR characterization of [Ru([9]aneS_3)Cl(cppH)]$^+$ (**10**) in D_2O.
Figures S16-S20. NMR characterization of [Ru([9]aneS_3)Cl(cppH-RRPYIL)]$^+$ (**11**) in DMSO-d_6 and D_2O.
Figure S21. Comparison of the ^{1}H NMR spectra in D_2O (region of the aromatic Tyr protons) of **7**, **8**, and **11**.
Figure S22-S30. NMR characterization of cppH-RRPYIL in DMSO-d_6, D_2O, and CD_3OD.
Figure S31-34. Analytical HPLC chromatograms for *trans,cis*-$RuCl_2(CO)_2$(cppH-RRPYIL) (**7**), [Ru([9]aneS_3)(cppH-RRPYIL)(PTA)]$^{2+}$ (**8**), [Ru([9]aneS_3)Cl(cppH-RRPYIL)]$^+$ (**11**) and cppH-RRPYIL.

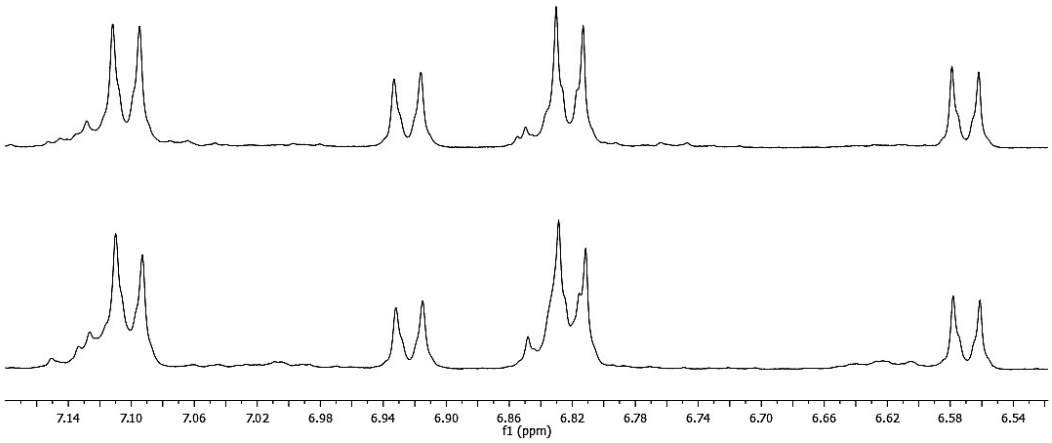

Figure S1. ^{1}H NMR spectra in D_2O (region of the aromatic protons of Tyr) of bio-conjugate **7** obtained 1) by reaction (using SPPS) between *trans*,*cis*-$RuCl_2(CO)_2$(cppH-κN^o) and RRPYIL (top), and 2) by the reaction in solution between *trans,cis,cis*-$RuCl_2(CO)_2$(dmso-O)$_2$ and cppH-RRPYIL (bottom).

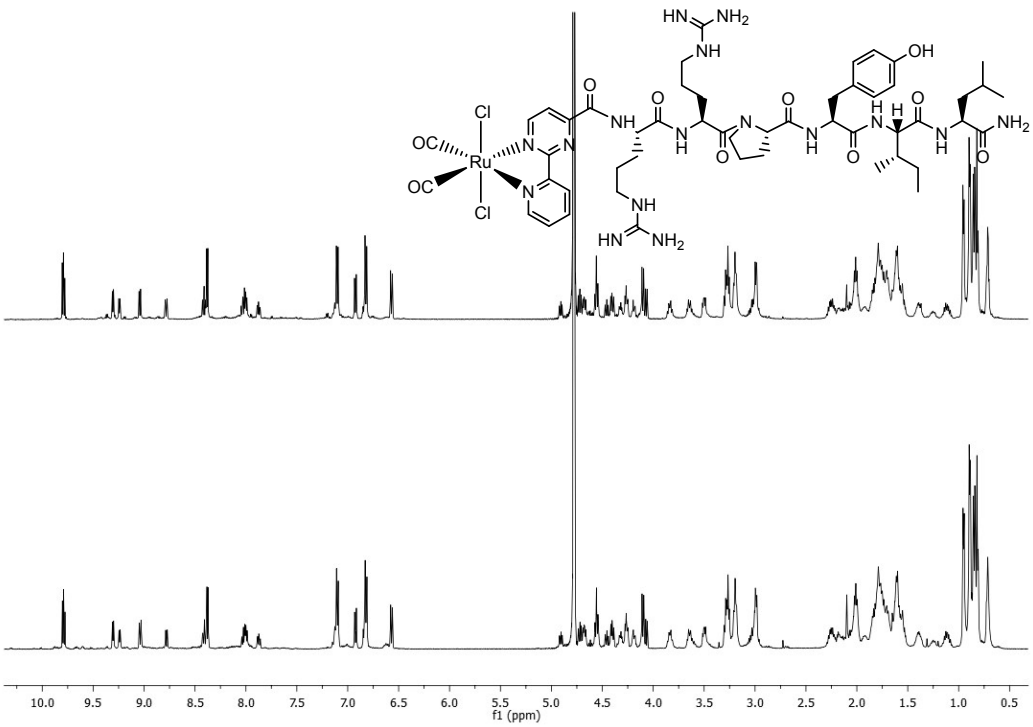

Figure S2. ^{1}H NMR spectra in D_2O of bio-conjugate **7** obtained 1) by reaction (using SPPS) between *trans*,*cis*-$RuCl_2(CO)_2$(cppH-κ*N*^{o}) and RRPYIL (top), and 2) by the reaction in solution between *trans,cis,cis*-$RuCl_2(CO)_2$(dmso-O)$_2$ and cppH-RRPYIL (bottom).

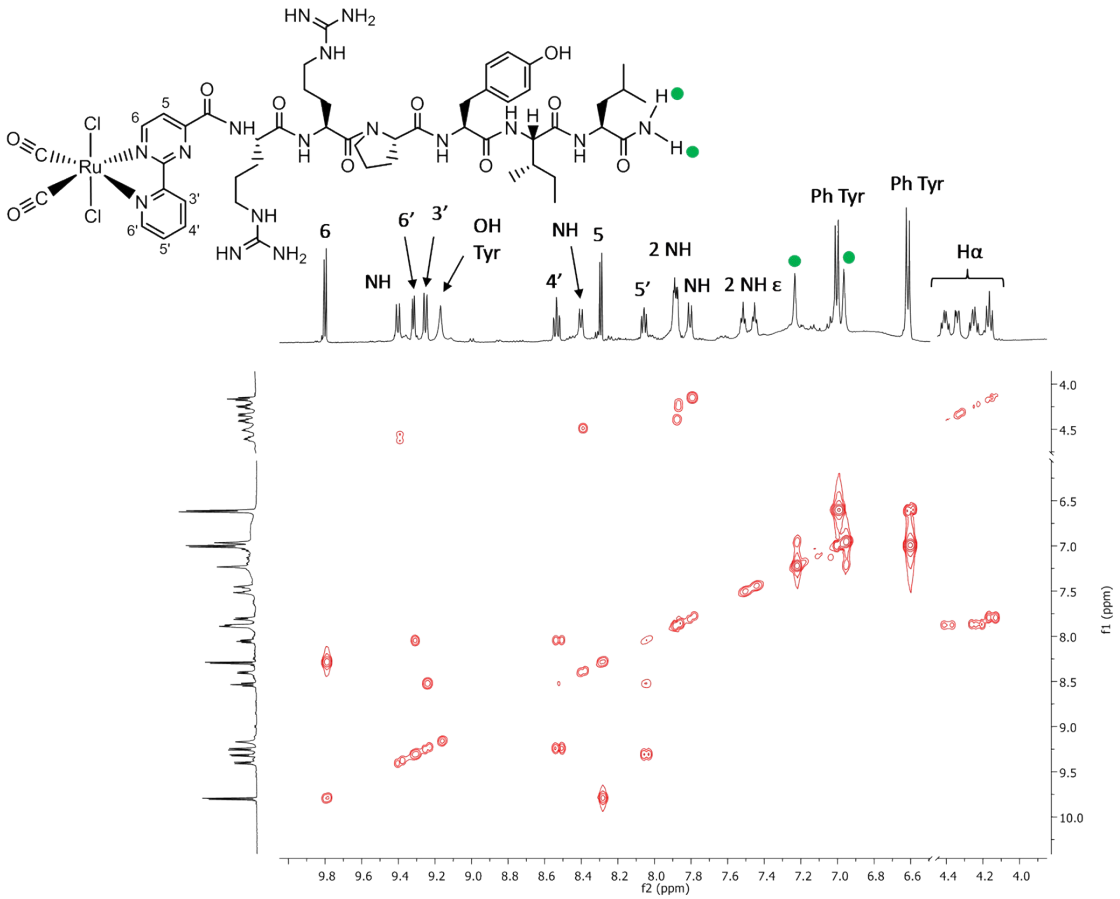

Figure S3. ^{1}H-^{1}H COSY spectrum in DMSO-d_6 of *trans,cis*-$RuCl_2(CO)_2$(cppH-RRPYIL) (**7**) (selected regions). NH indicates the amidic protons of the peptide.

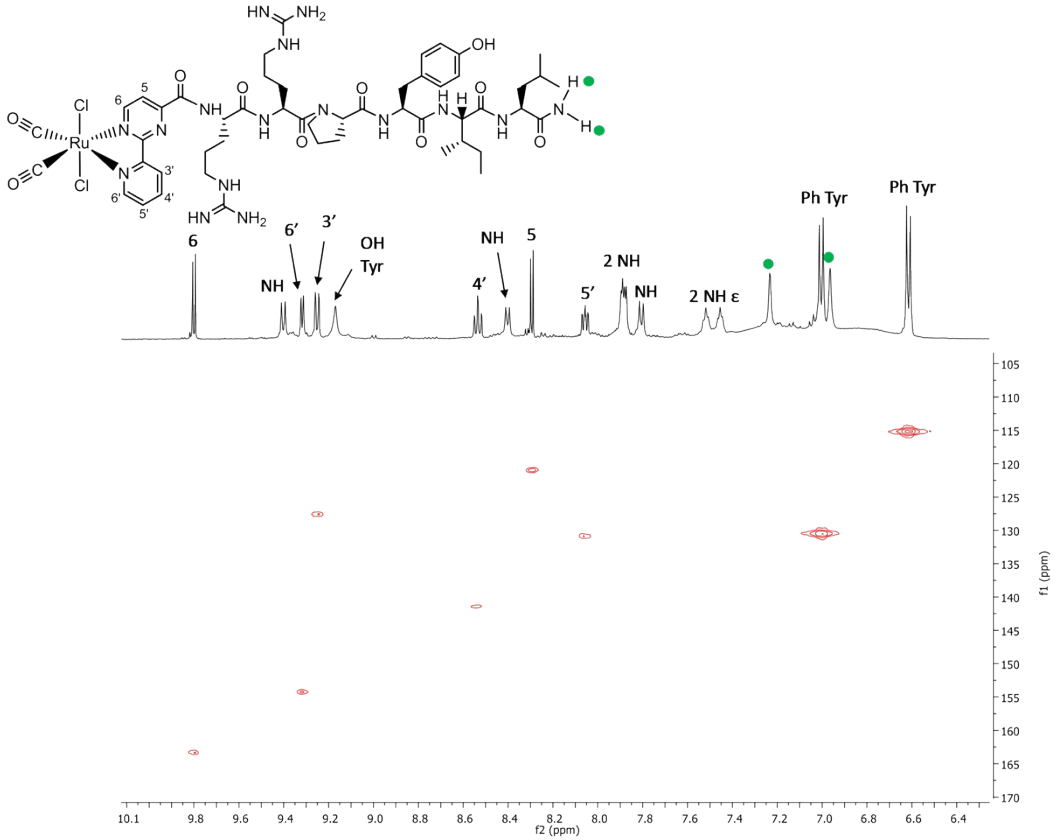

Figure S4. Aromatic region of the ^{1}H-^{13}C HSQC NMR spectrum in DMSO-d_6 of *trans,cis*-$RuCl_2(CO)_2$(cppH-RRPYIL) (**7**). NH indicates the amidic protons of the peptide.

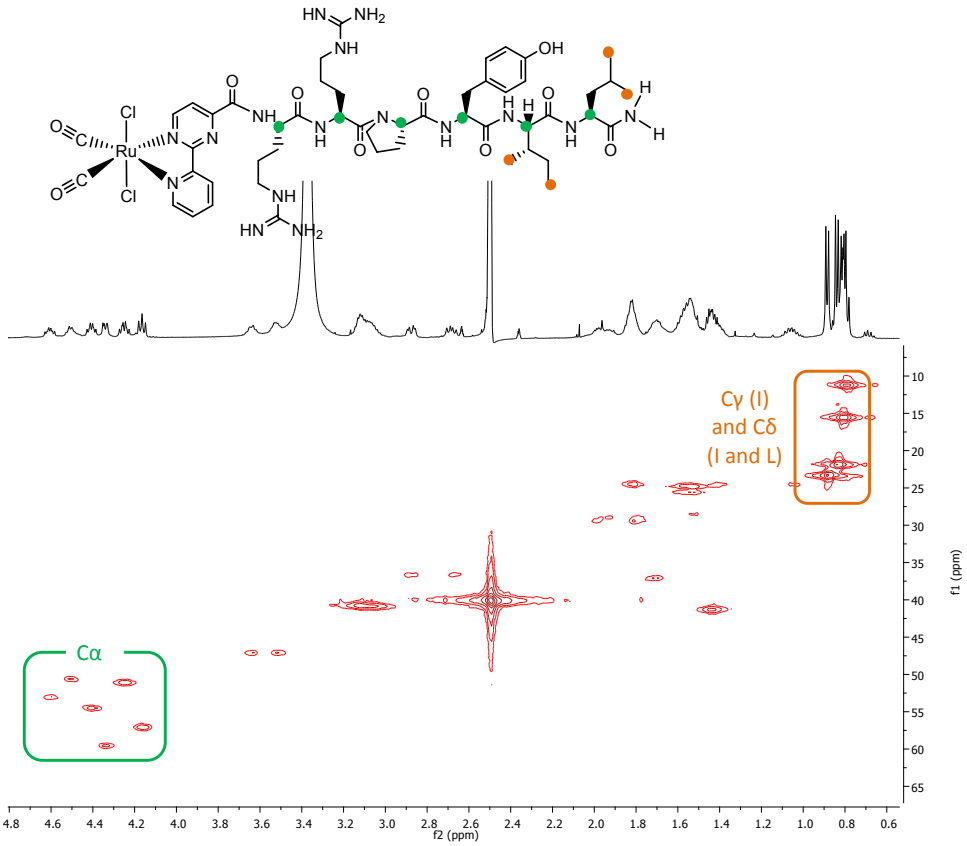

Figure S5. Aliphatic region of the ^{1}H-^{13}C HSQC NMR spectrum in DMSO-d_6 of *trans,cis*-$RuCl_2(CO)_2$(cppH-RRPYIL) (**7**).

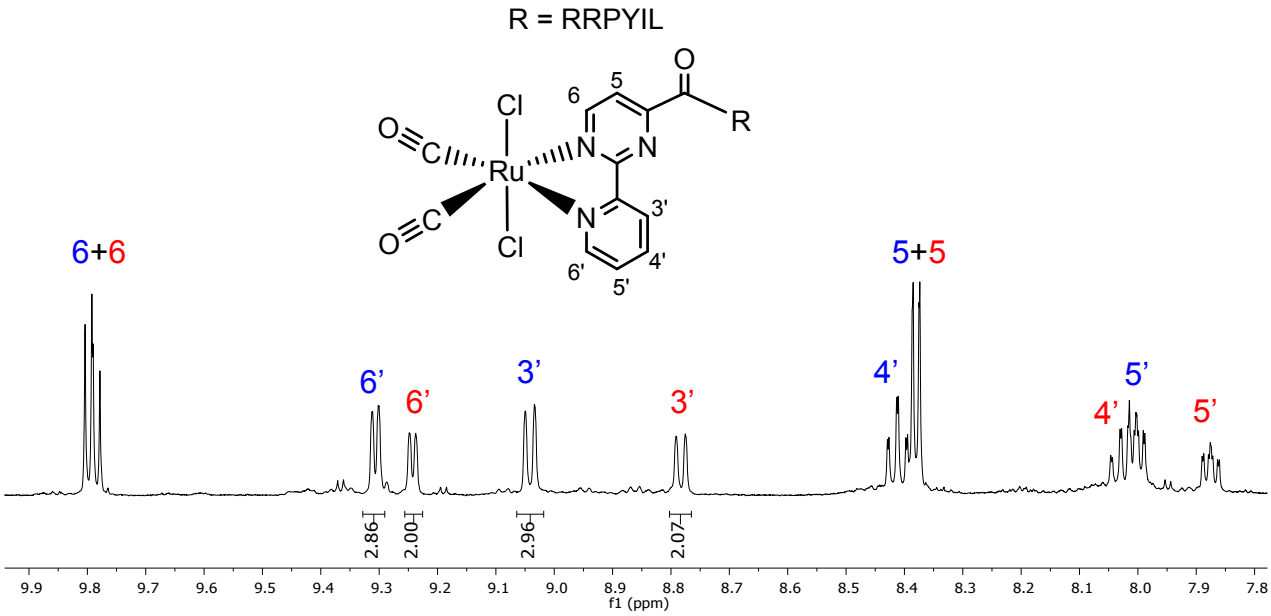

Figure S6. Aromatic region of the ^{1}H NMR spectrum of **7** in D_2O, with the integrals for the resonances of protons 3′ and 6′(blue labels for the major isomer, red for the minor one).

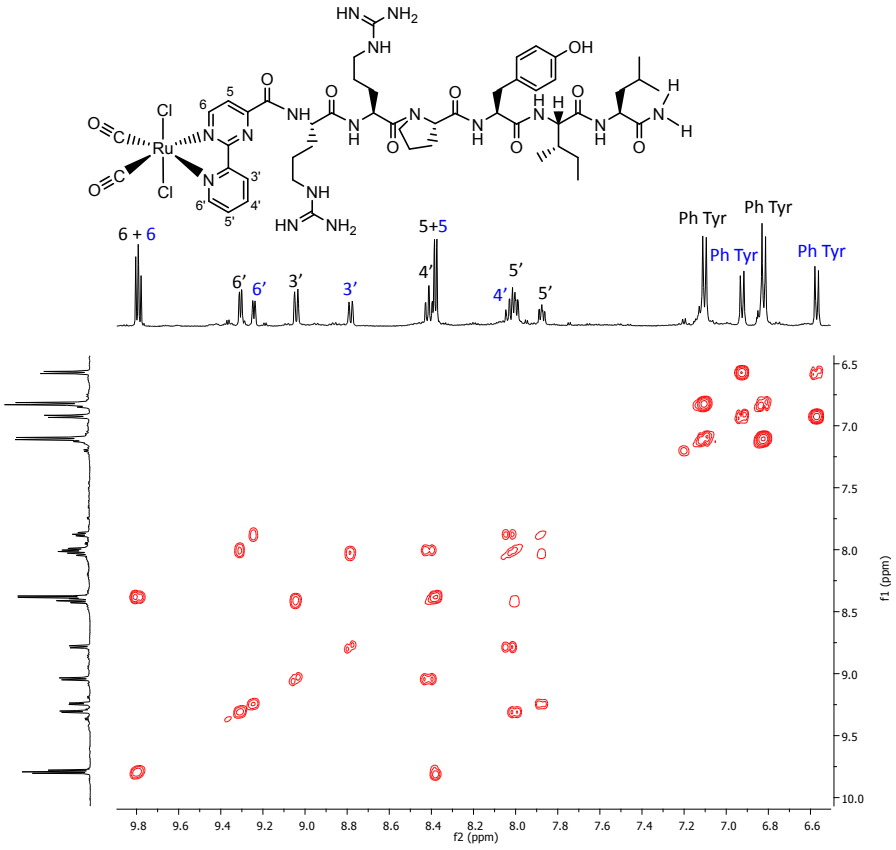

Figure S7. ^{1}H-^{1}H COSY in D_2O (aromatic region) of *trans,cis*-$RuCl_2(CO)_2$(cppH-RRPYIL) (**7**).

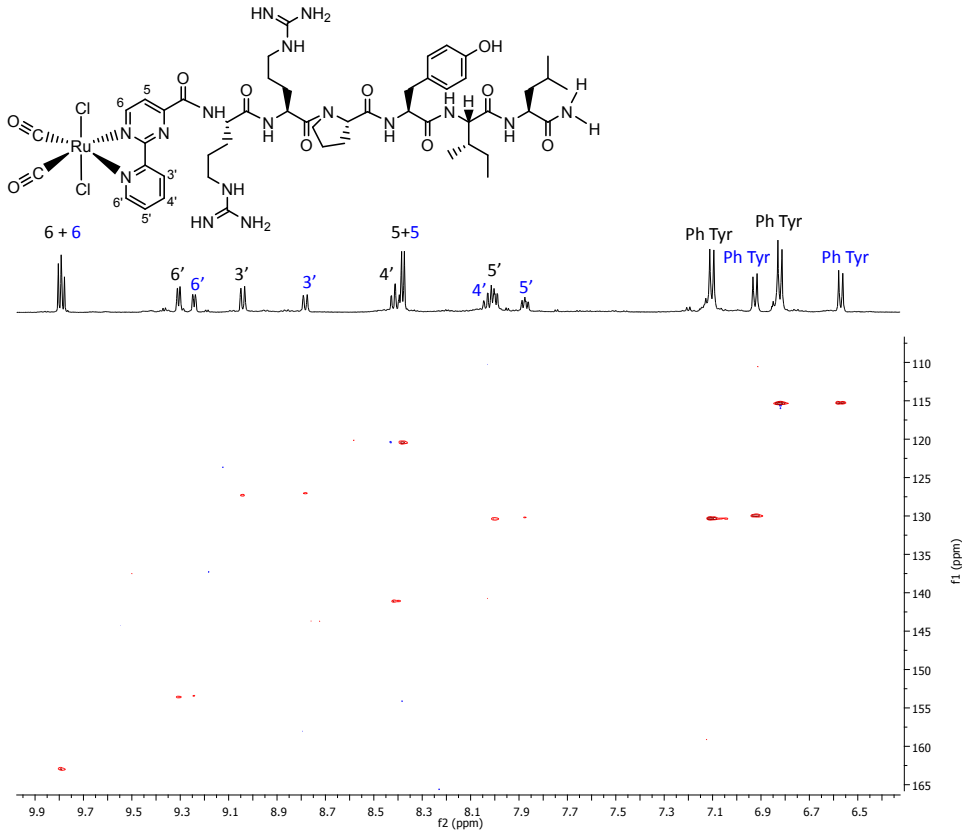

Figure S8. ^{1}H-^{13}C HSQC NMR spectrum in D_2O (aromatic region) of *trans,cis*-$RuCl_2(CO)_2$(cppH-RRPYIL) (**7**).

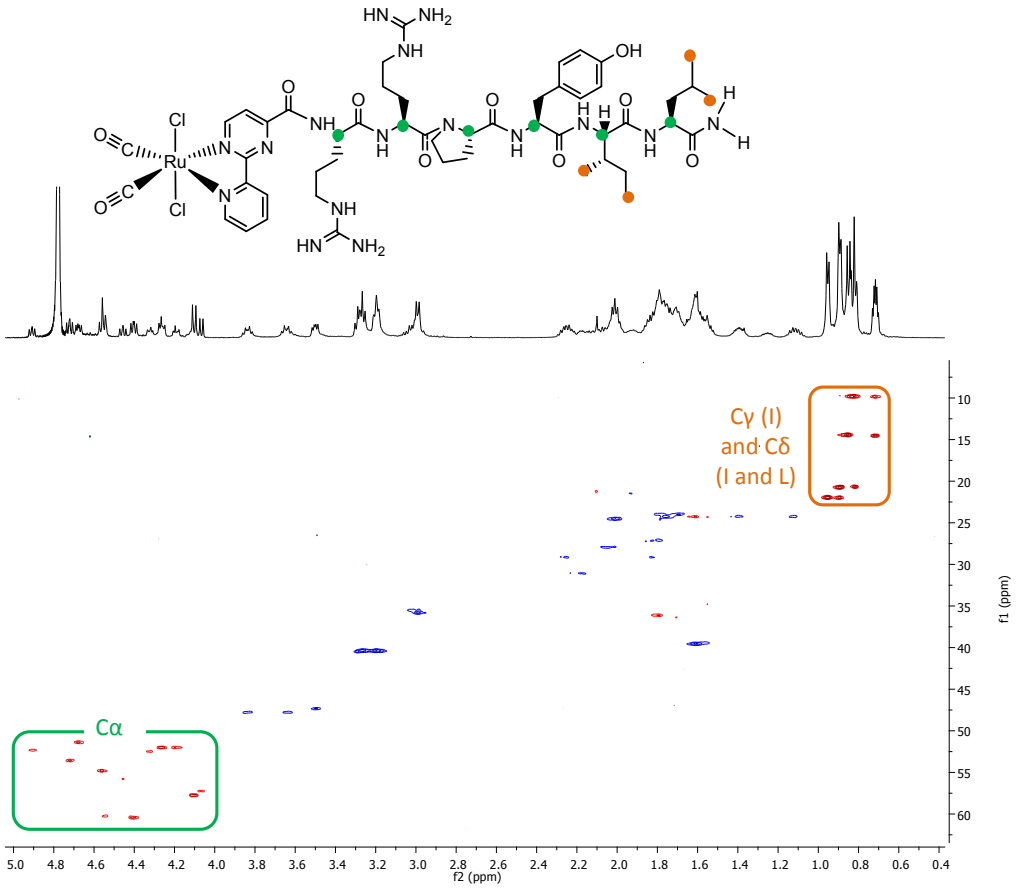

Figure S9. ^{1}H-^{13}C HSQC NMR spectrum in D_2O (aliphatic region) of *trans,cis*-$RuCl_2(CO)_2$(cppH-RRPYIL) (**7**).

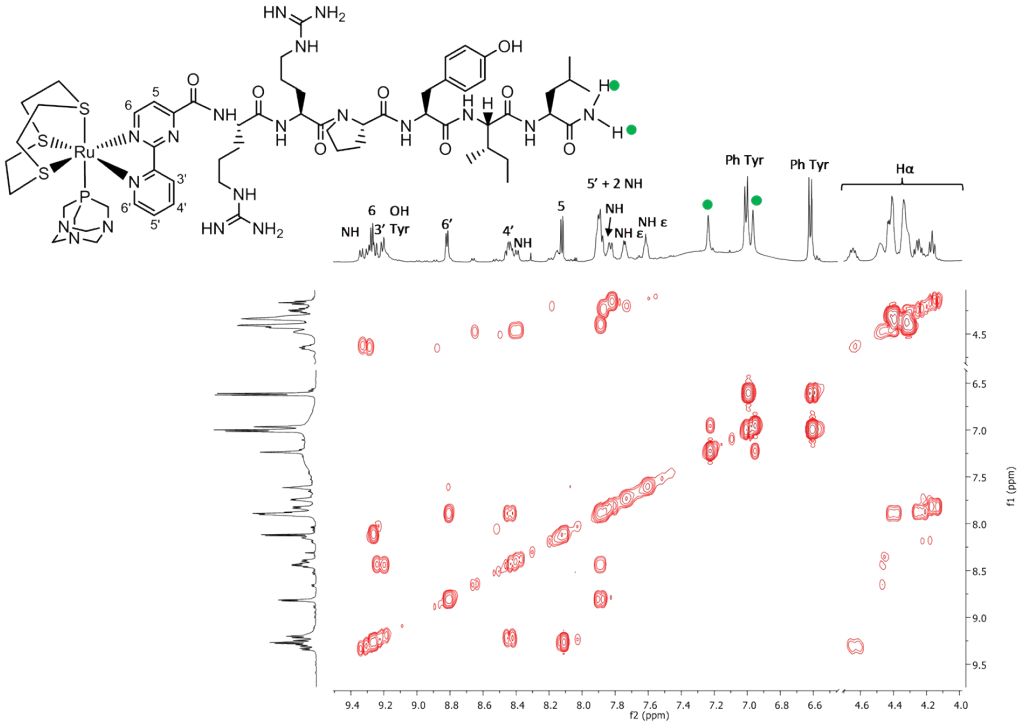

Figure S10. ^{1}H-^{1}H COSY NMR spectrum in DMSO-d_6 (selected regions) of [Ru([9]aneS$_3$)(cppH-NT)(PTA)]$^{2+}$ (**8**). NH indicates the amidic protons of the peptide.

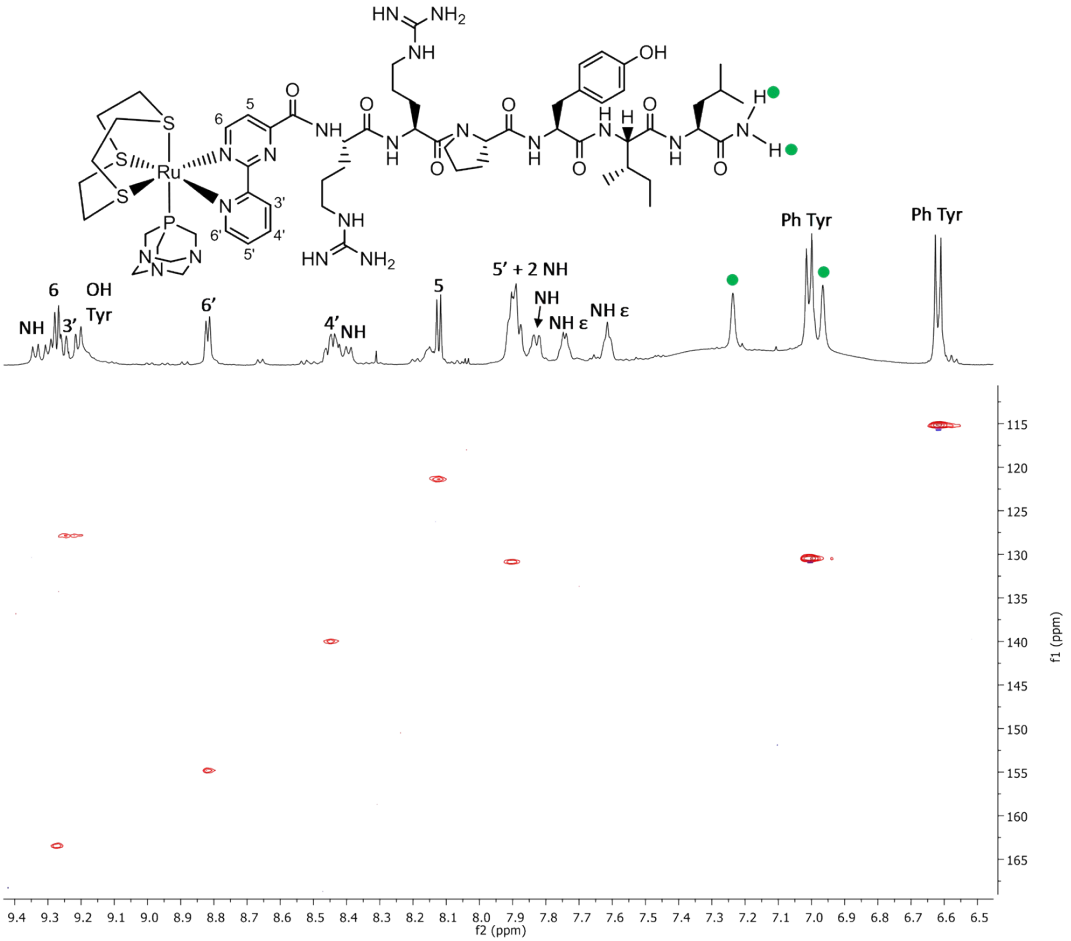

Figure S11. ^{1}H-^{13}C HSQC NMR spectrum in DMSO-d_6 (aromatic region) of [Ru([9]aneS$_3$)(cppH-NT)(PTA)]$^{2+}$ (**8**). NH indicates the amidic protons of the peptide.

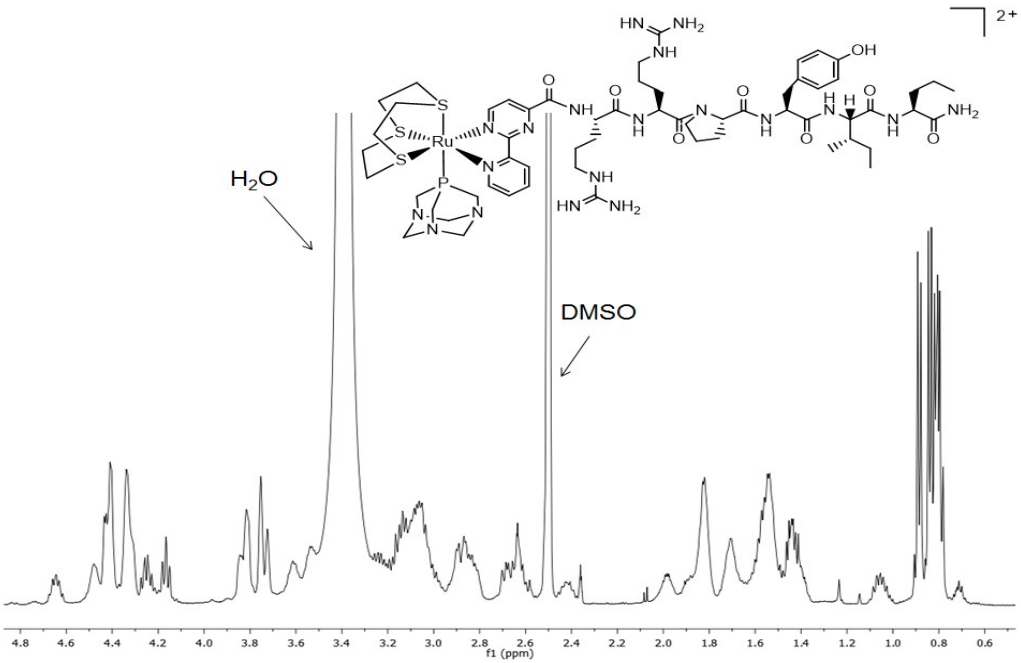

Figure S12. Upfield region of the ^{1}H NMR spectrum in DMSO-d_6 of [Ru([9]aneS_3)(cppH-NT)(PTA)]$^{2+}$ (**8**).

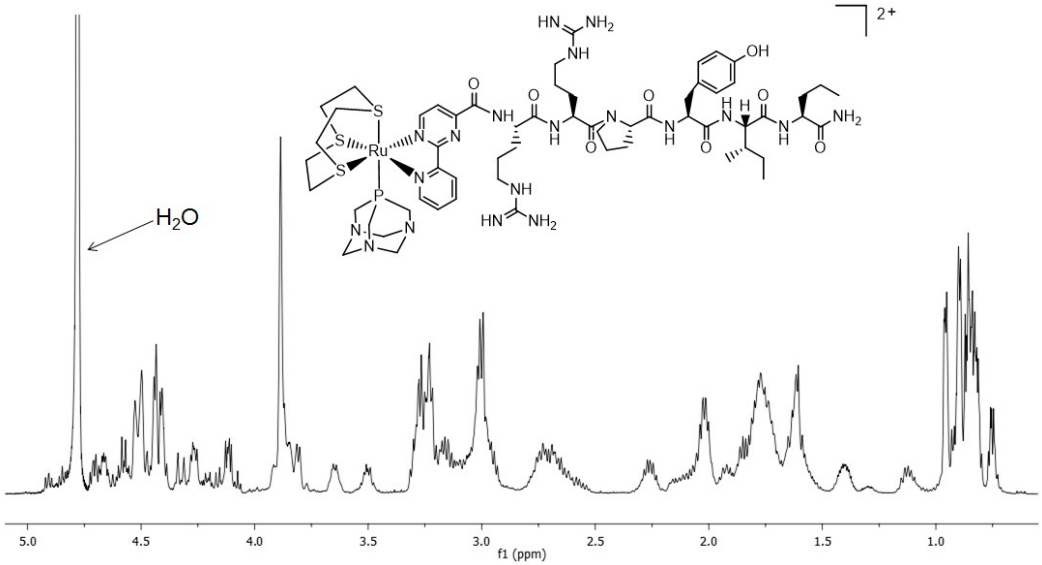

Figure S13. Upfield region of the ^{1}H NMR spectrum in D_2O of $[Ru([9]aneS_3)(cppH\text{-}NT)(PTA)]^{2+}$ (**8**).

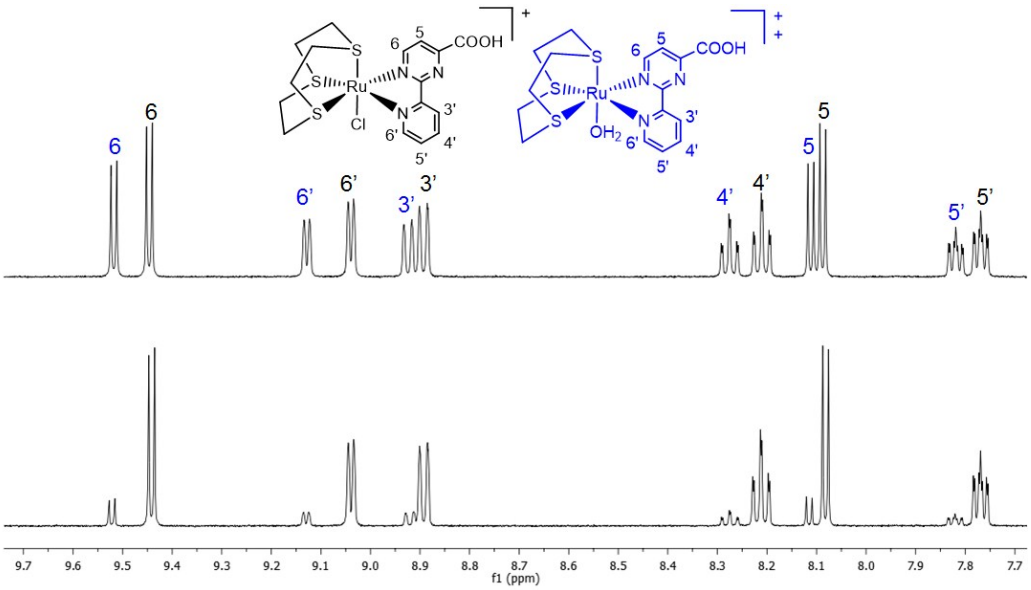

Figure S14. ^{1}H NMR spectra in D_2O of the model complex [Ru([9]aneS_3)Cl(cppH)]Cl (**10**) after dissolution in D_2O (top) and after addition of an excess of NaCl (bottom).

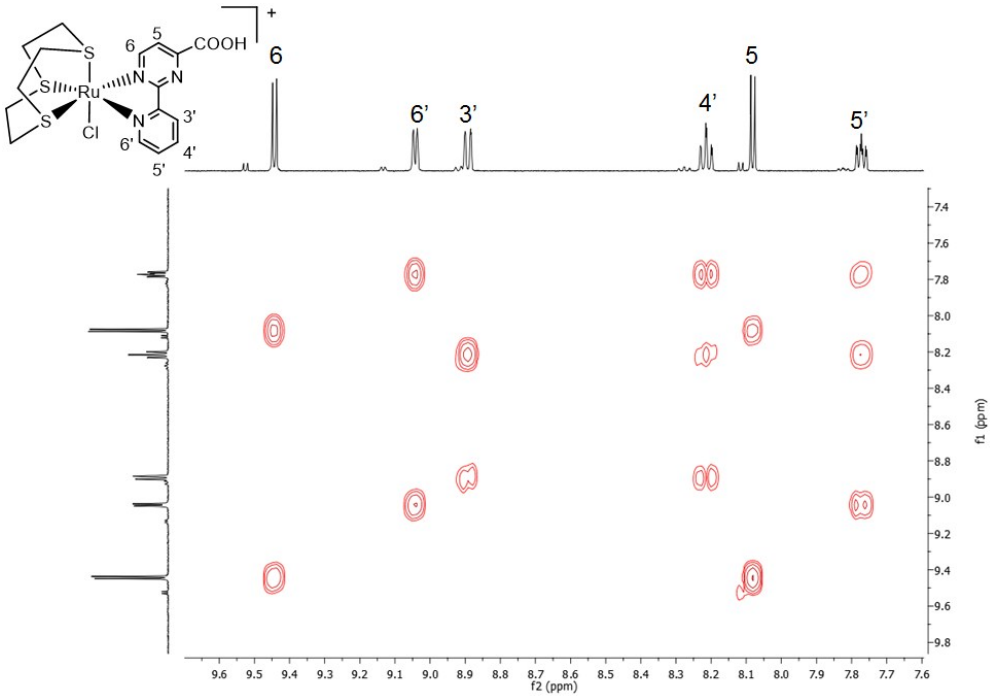

Figure S15. ^{1}H-^{1}H COSY NMR spectrum in D_2O + NaCl of the model complex [Ru([9]aneS_3)Cl(cppH)]Cl (**10**).

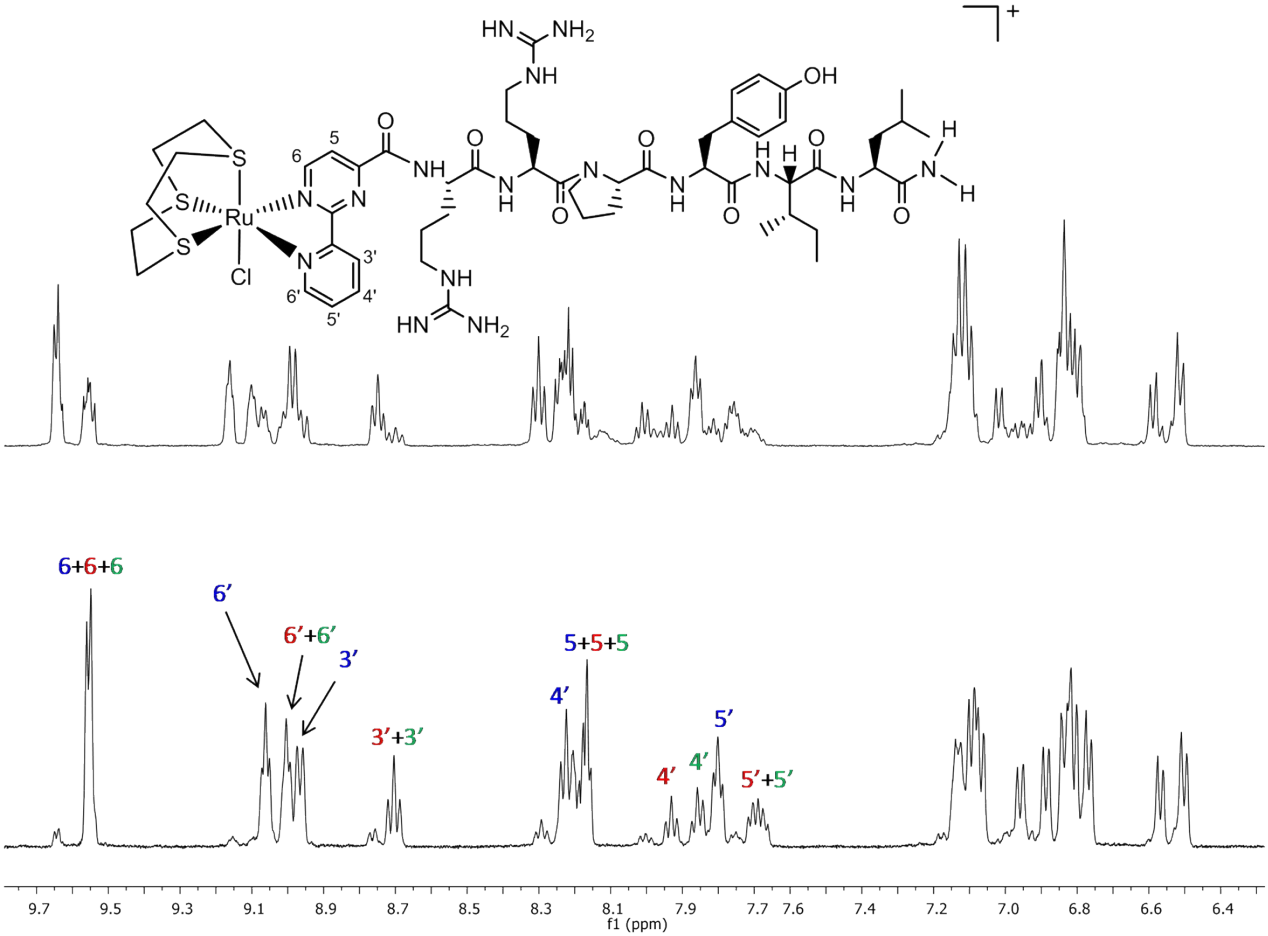

Figure S16. ^{1}H NMR spectra (aromatic region) of [Ru([9]aneS$_3$)Cl(cppH-RRPYIL)]$^{+}$ (**11**) after dissolution in D_2O (top) and after addition of an excess of NaCl (bottom) to the same solution.

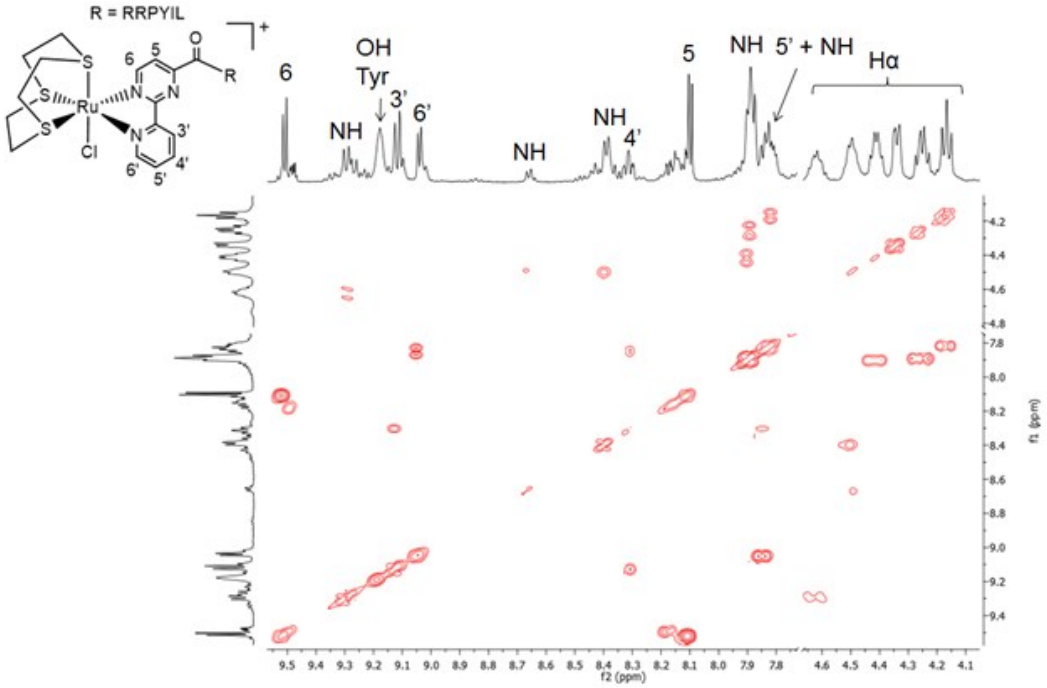

Figure S17. ^{1}H-^{1}H COSY NMR spectrum in DMSO-d_6 (selected regions) of [Ru([9]aneS$_3$)Cl(cppH-NT)]$^{+}$ (**11**). NH indicates the amidic protons of the peptide.

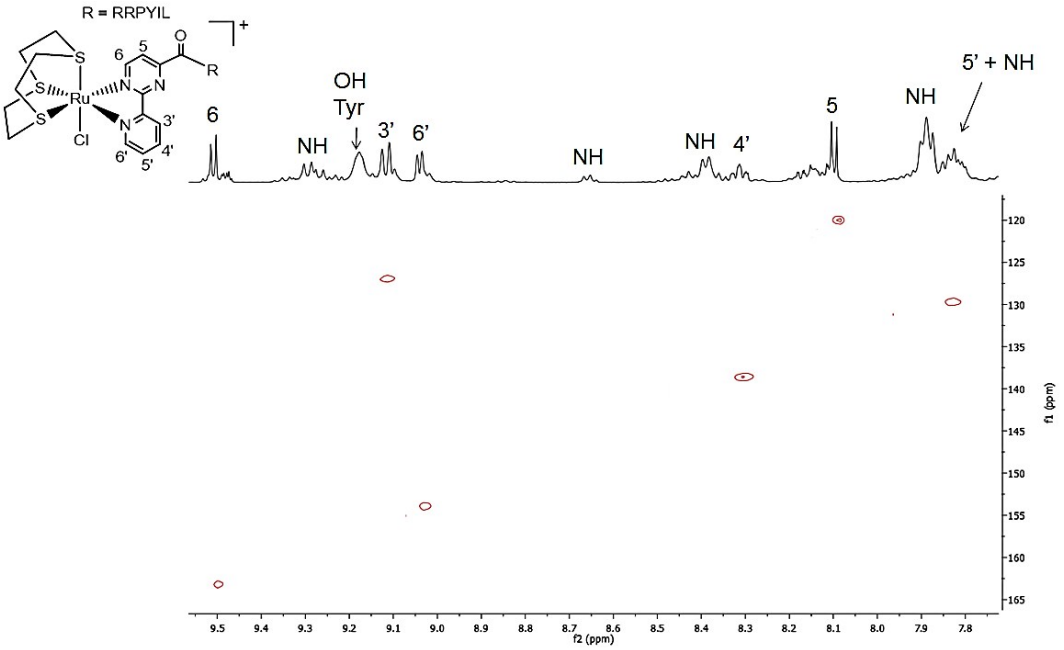

Figure S18. ^{1}H-^{13}C HSQC NMR spectrum in DMSO-d_6 (aromatic region) of $[Ru([9]aneS_3)Cl(cppH\text{-}NT)]^+$ (**11**). NH indicates the amidic protons of the peptide.

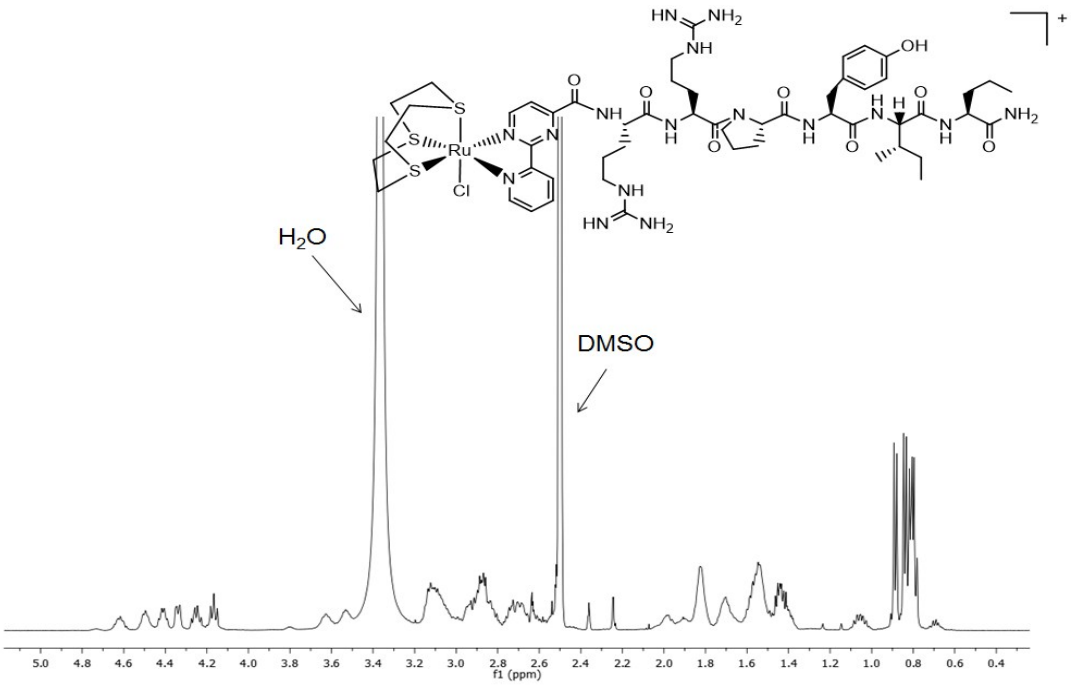

Figure S19. Upfield region of the ^{1}H NMR spectrum in DMSO-d_6 of [Ru([9]aneS$_3$)Cl(cppH-RRPYIL)]$^{+}$ (**11**).

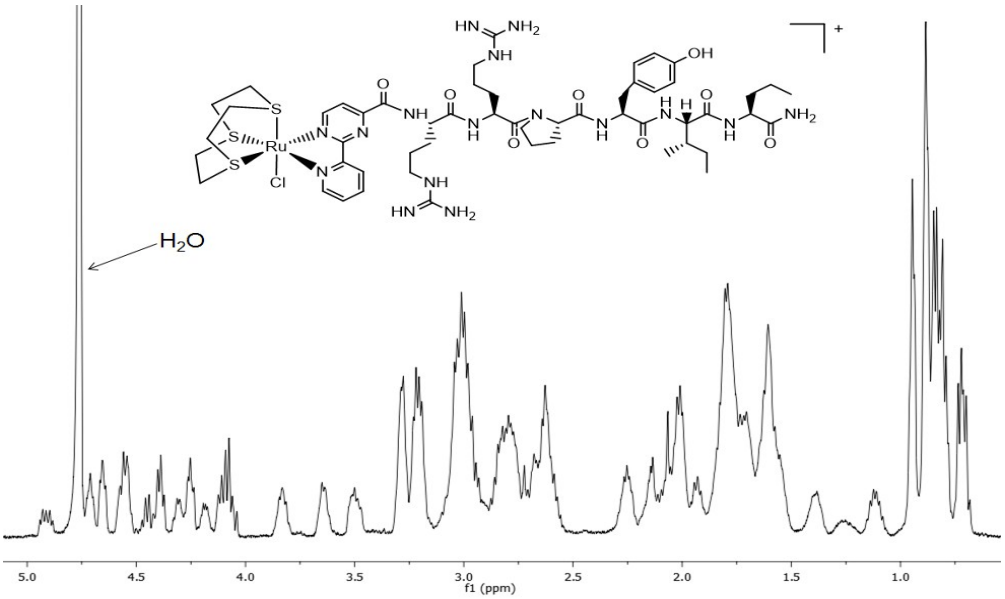

Figure S20. Upfield region of the ^{1}H NMR spectrum in D_2O of $[Ru([9]aneS_3)Cl(cppH\text{-}RRPYIL)]^{+}$ (**11**).

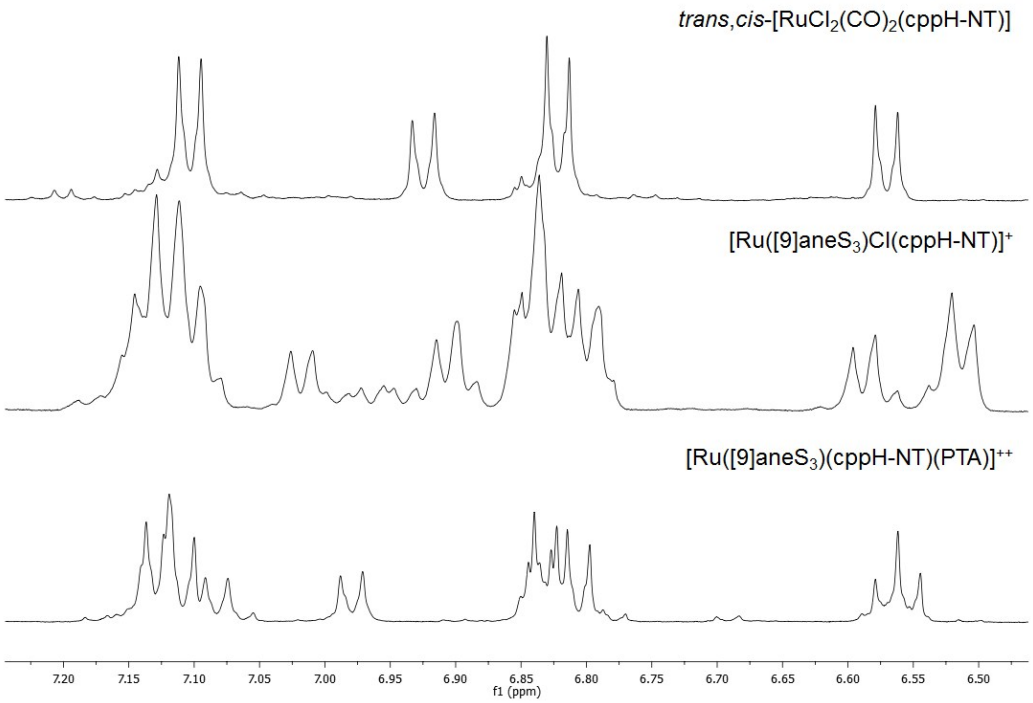

Figure S21. ^{1}H NMR spectra in D_2O (region of the aromatic Tyr protons) of **7** (top), **11** (middle, in D_2O + NaCl), and **8** (bottom).

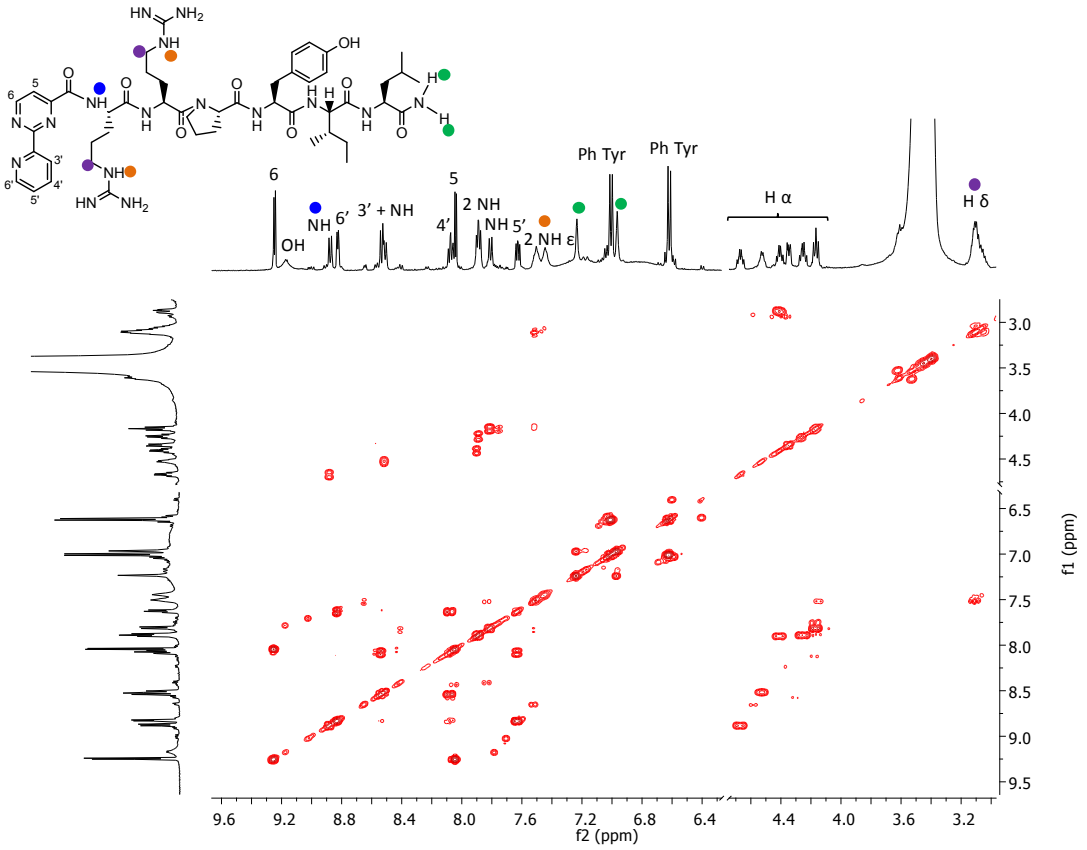

Figure S22. ^{1}H-^{1}H COSY NMR spectrum in DMSO-d_6 of cppH-RRPYIL (selected regions). NH indicates the amidic protons of the peptide.

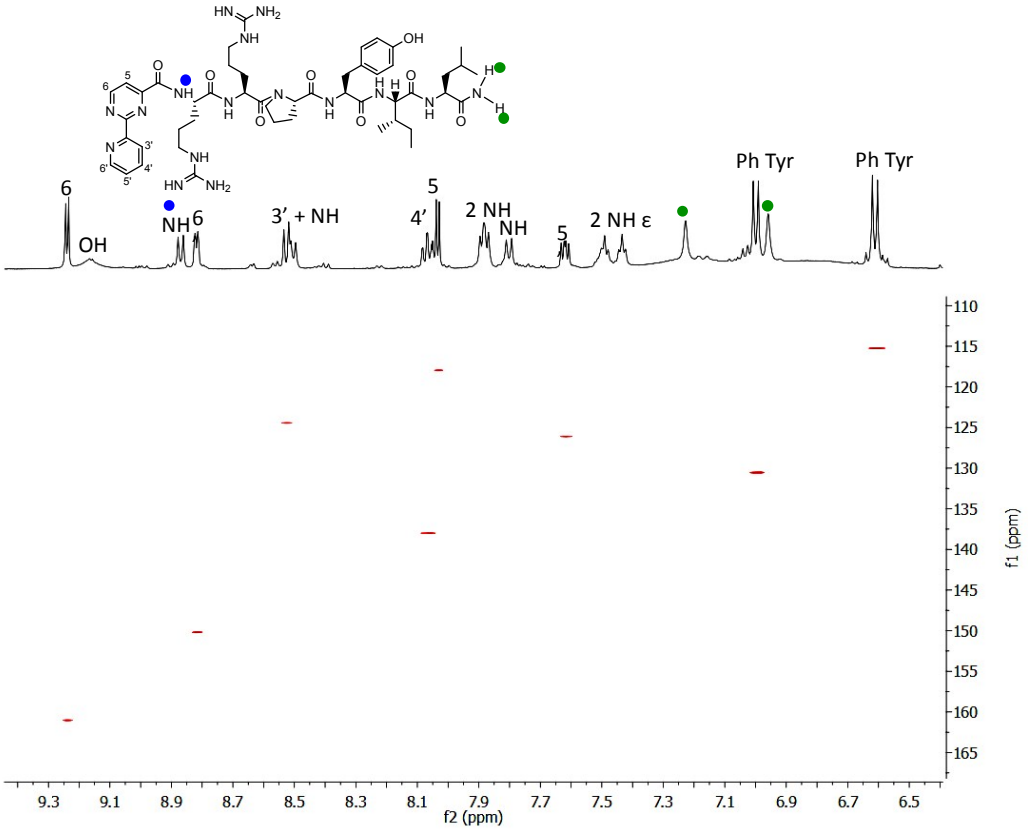

Figure S23. ^{1}H-^{13}C HSQC NMR spectrum in DMSO-d_6 (aromatic region) of cppH-RRPYIL. NH indicates the amidic protons of the peptide.

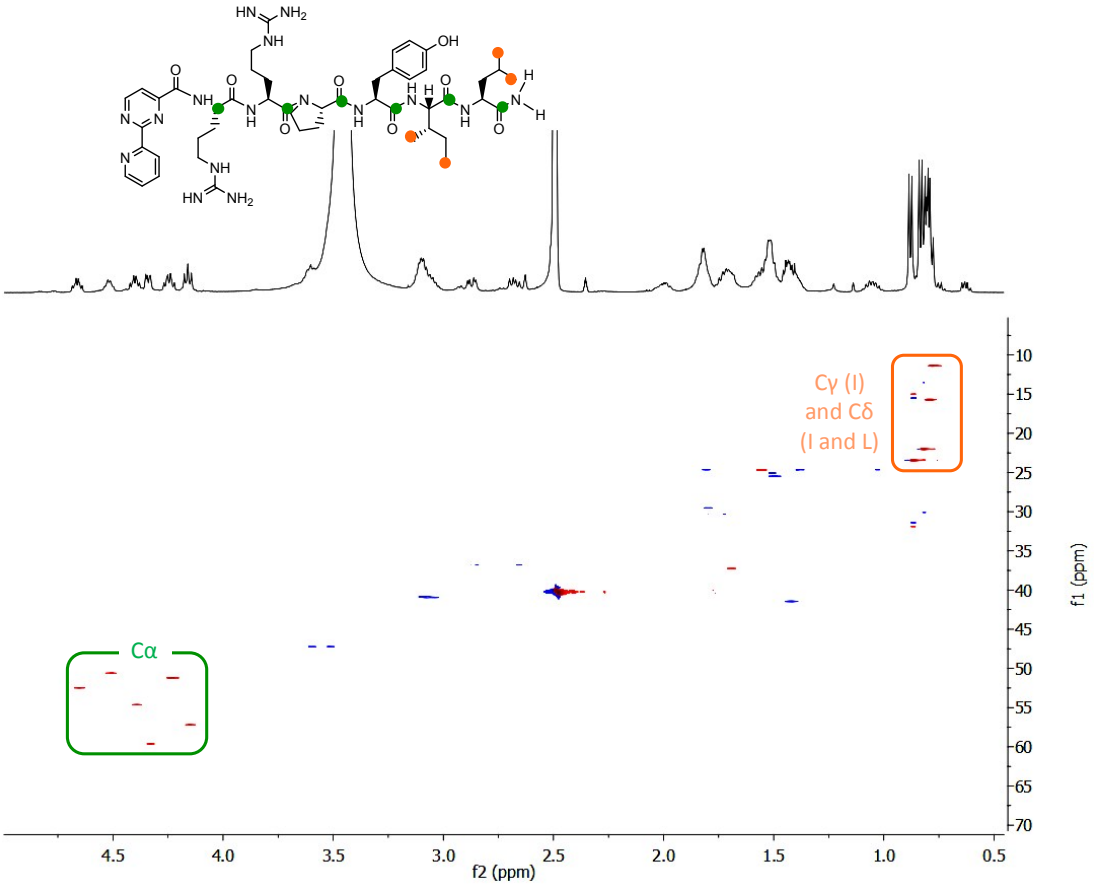

Figure S24. ^{1}H-^{13}C HSQC NMR spectrum in DMSO-d_6 (aliphatic region) of cppH-RRPYIL.

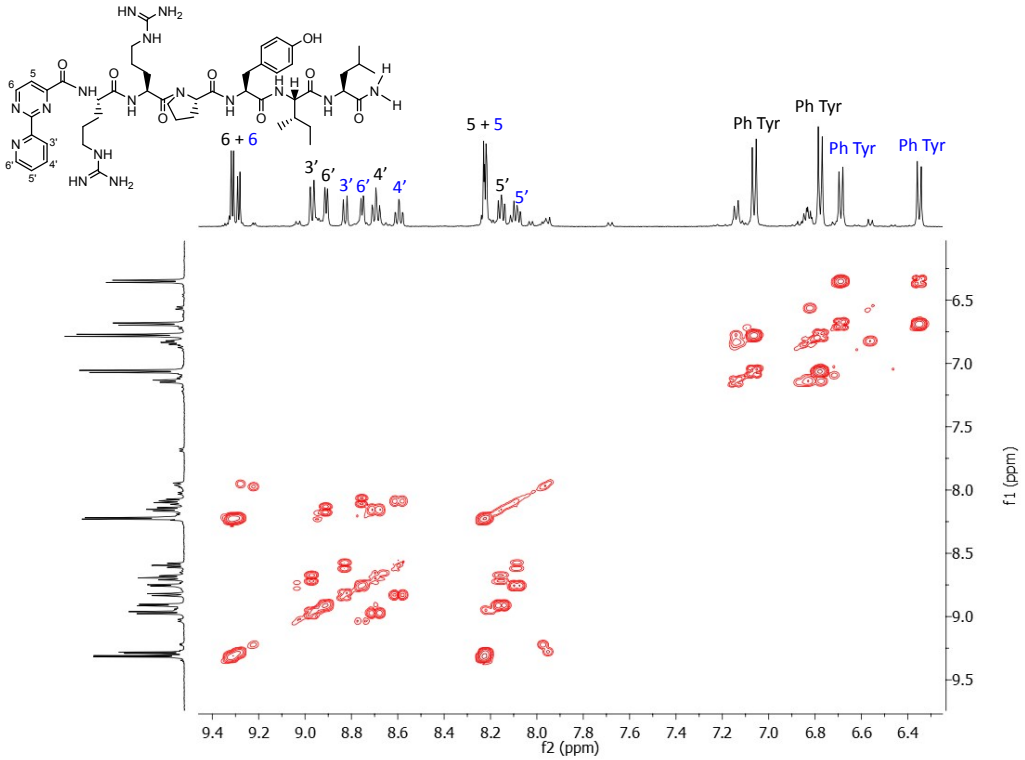

Figure S25. ^{1}H-^{1}H COSY NMR spectrum in D_2O (aromatic region) of cppH-RRPYIL.

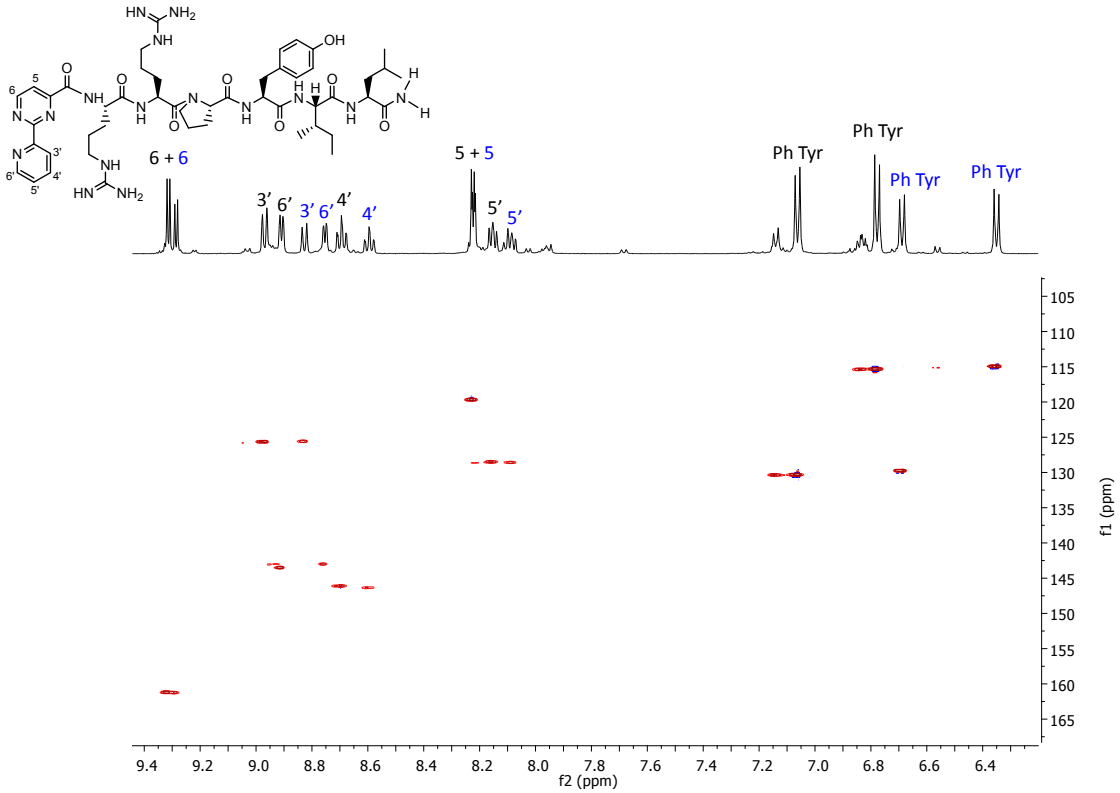

Figure S26. ^{1}H-^{13}C HSQC NMR spectrum in D_2O (aromatic region) of cppH-RRPYIL.

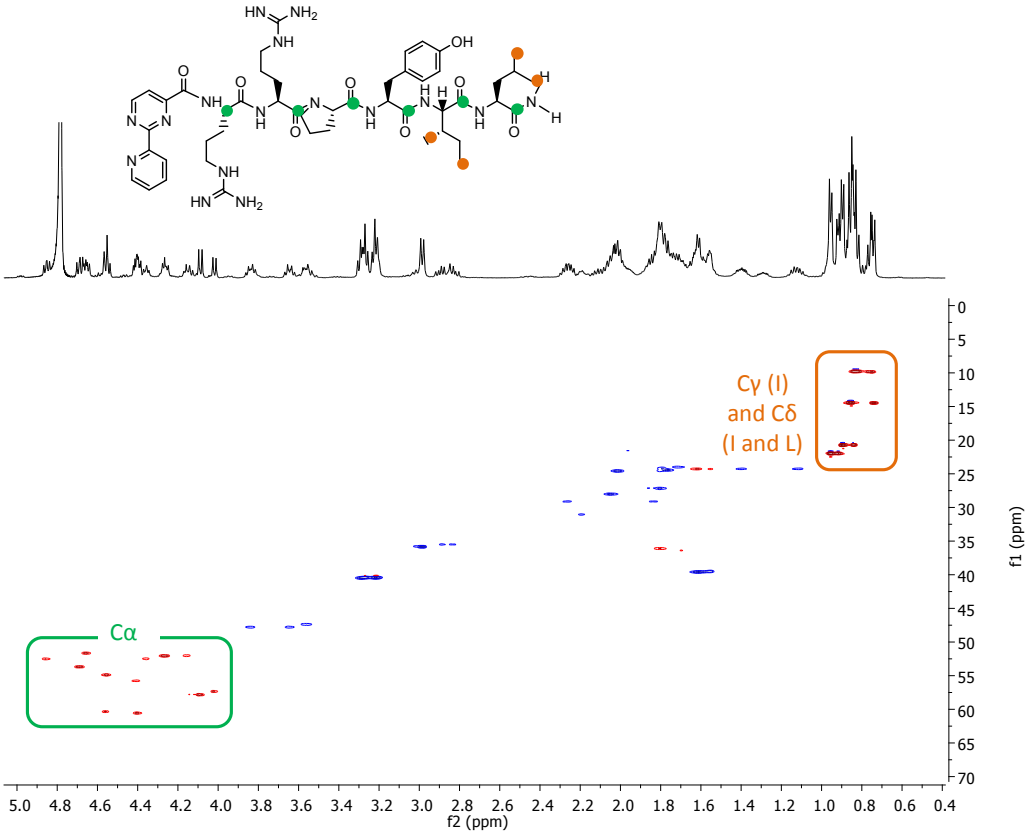

Figure S27. ^{1}H-^{13}C HSQC NMR spectrum in D_2O (aliphatic region) of cppH-RRPYIL.

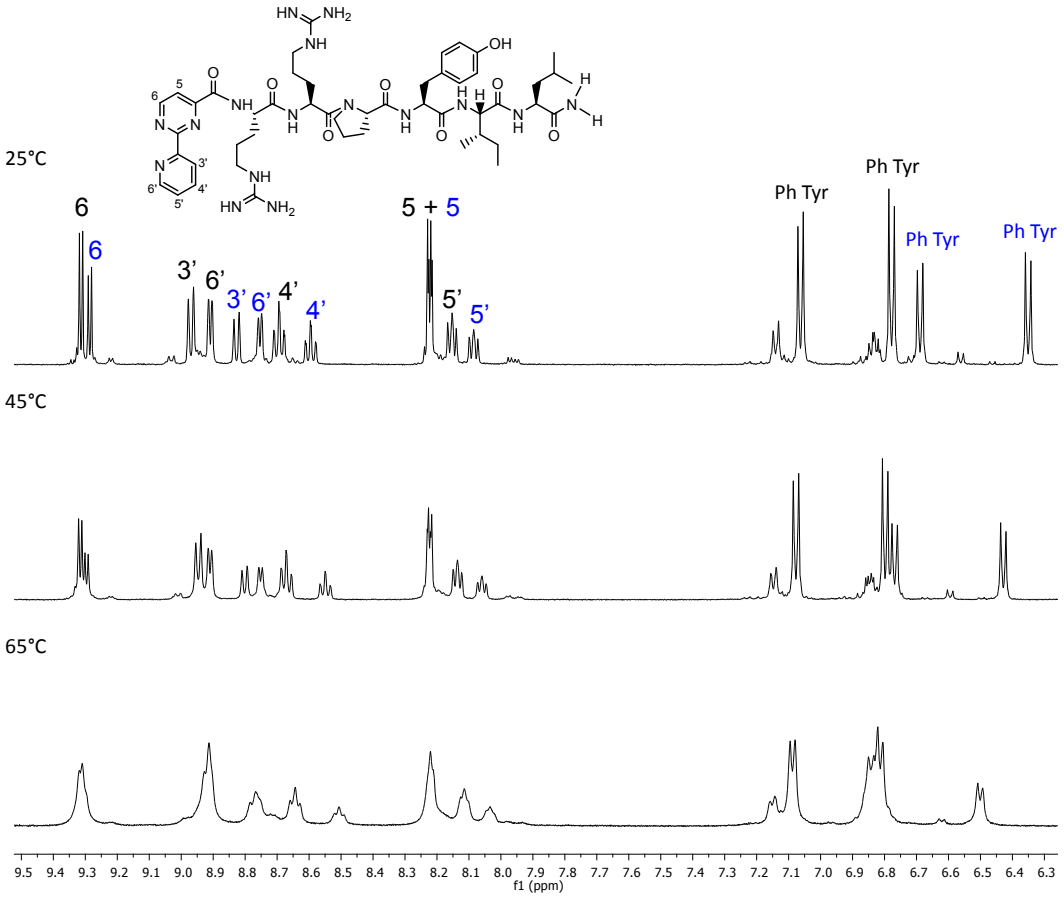

Figure S28. ^{1}H NMR spectra (aromatic region) of cppH-RPPYIL recorded at 25°C (top), 45°C (middle) and 65°C (bottom) in D_2O.

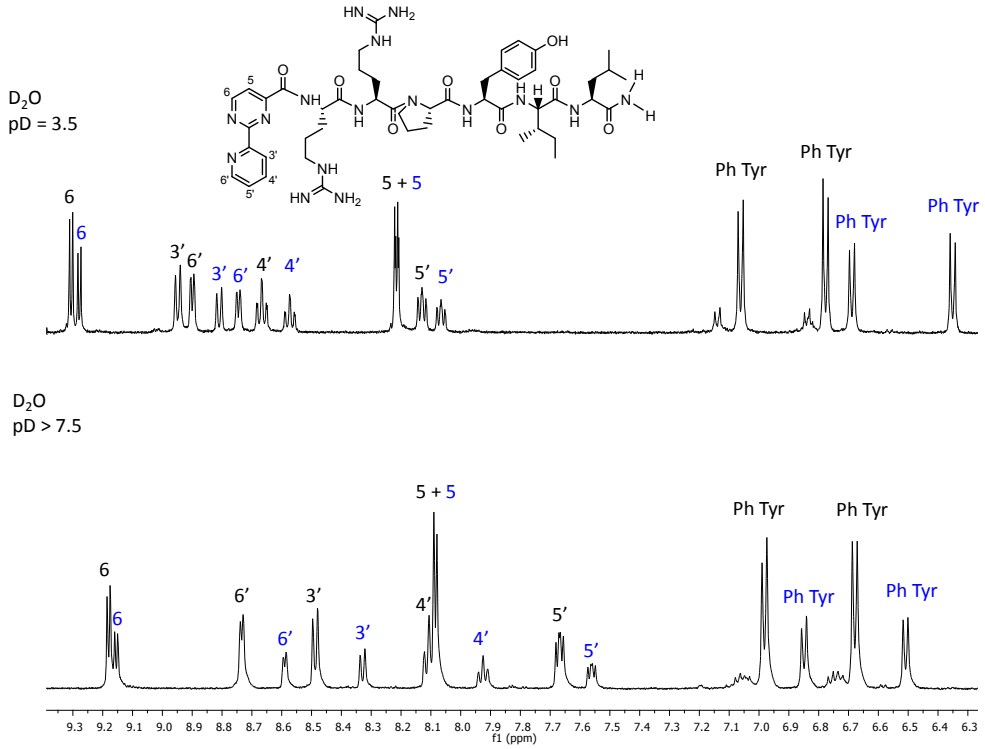

Figure S29. ^{1}H NMR spectra (aromatic region) of cppH-RPPYIL recorded at pD = 3.5 (top) and pD > 7.5 (bottom) in D_2O.

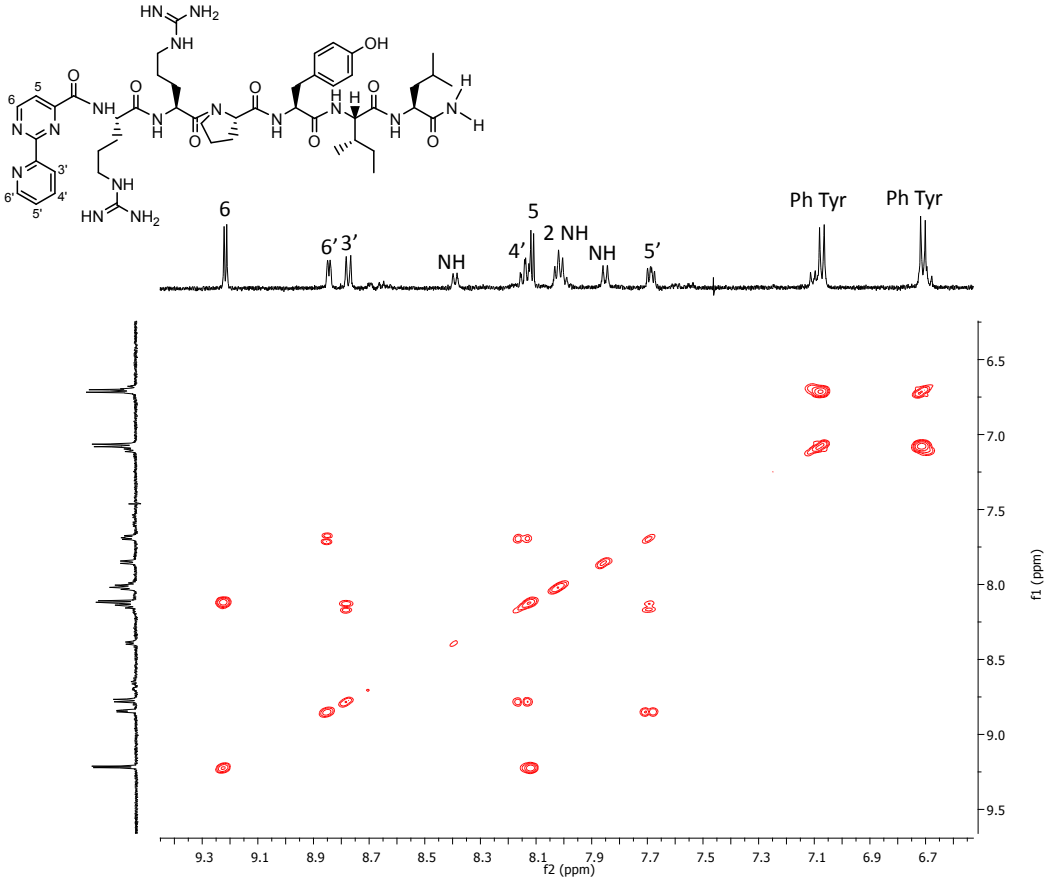

Figure S30. ^{1}H-^{1}H COSY NMR spectrum (aromatic region) of cppH-RRPYIL in CD_3OD.

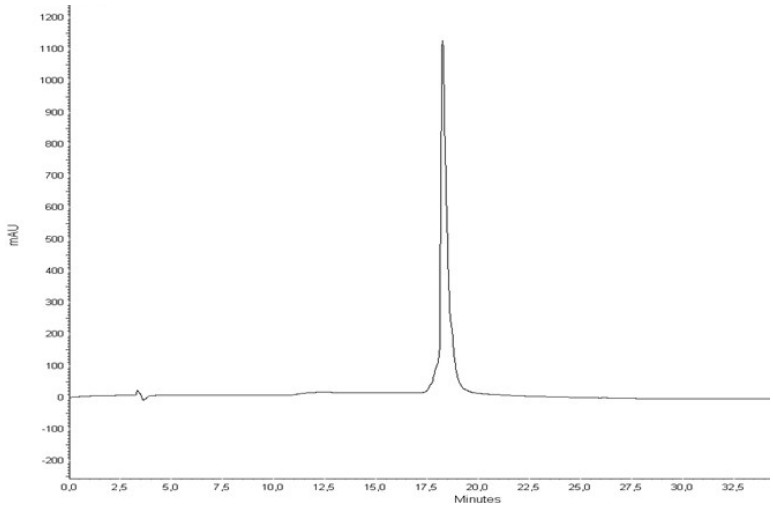

Figure S31. Analytical HPLC chromatogram of *trans,cis*-$RuCl_2(CO)_2$(cppH-RRPYIL) (**7**).

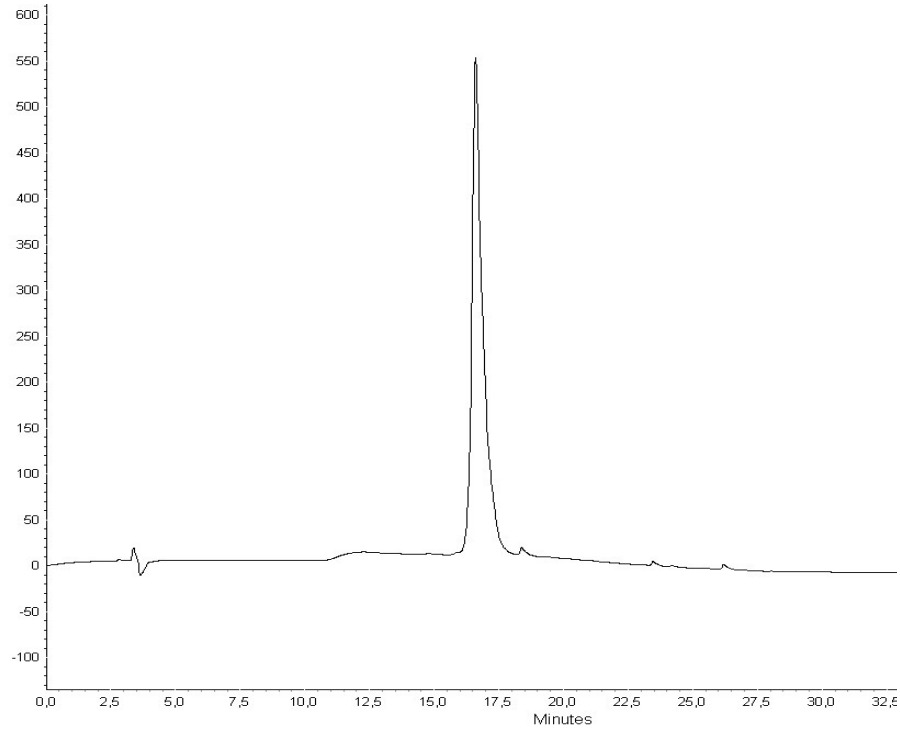

Figure S32. Analytical HPLC chromatogram of $[Ru([9]aneS_3)(cppH\text{-}RRPYIL)(PTA)]^{2+}$ (**8**).

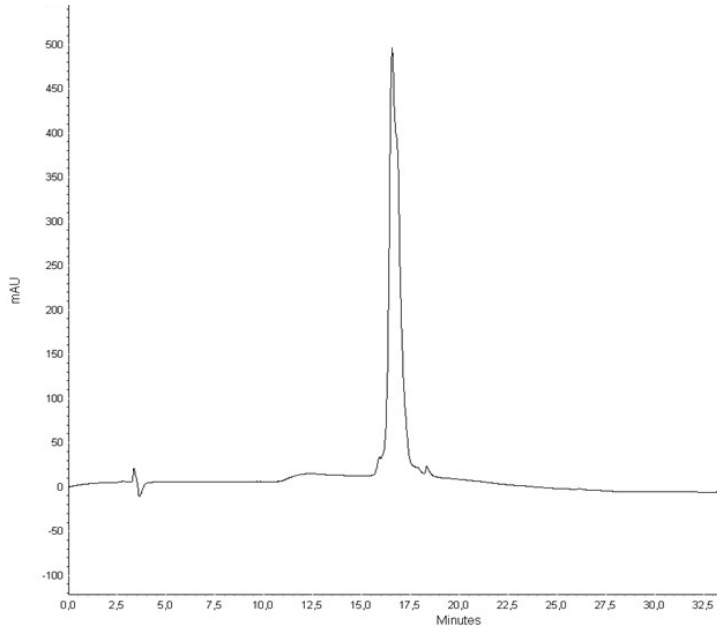

Figure S33. Analytical HPLC chromatogram of [Ru([9]aneS$_3$)Cl(cppH-RRPYIL)]$^+$ (**11**).

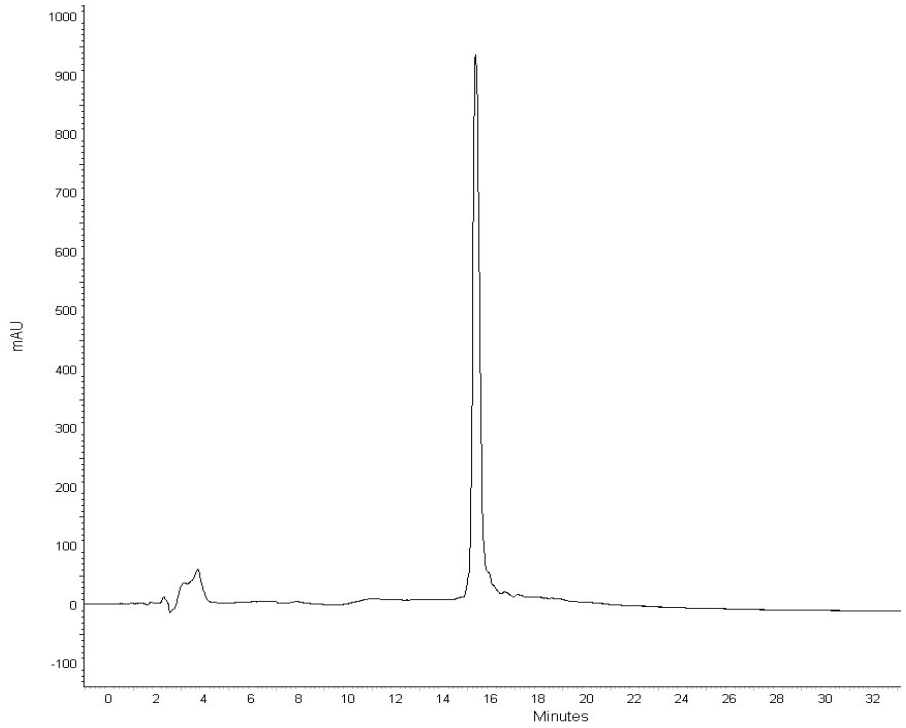

Figure S34. Analytical HPLC chromatogram of cppH-RRPYIL.

Table S1. Crystallographic data and refinement details for compound [Ru([9]aneS$_3$)Cl(cppH)]Cl ·0.45H$_2$O (**10**).

	10
Empirical Formula	$C_{16}H_{19}N_3Cl_2O_2S_3Ru \cdot 0.45H_2O$
Formula weight (Da)	561.85
Temperature (K)	100(2)
Wavelength (Å)	0.700
Crystal system	monoclinic
Space Group	*P* 21/c
a (Å)	17.795(2)
b (Å)	13.8510(8)
c (Å)	11.484(1)
α (°)	90
β (°)	104.985(15)
γ (°)	90
V (Å^3)	2734.3(5)
Z	4
ρ (g·cm^{-3})	1.3643
F(000)	1152
μ (mm^{-1})	0.961
θ min, max (°)	2.317, 30.977
Resolution (Å)	0.68
Total refl. collctd	98476
Independent refl.	8800
Obs. Refl. [Fo>4σ(Fo)]	8732
I/σ(I) (all data)	77.73
I/σ(I) (max res)	34.73
Completeness (all data)	0.950
R_{merge} (all data)	2.2%
R_{merge} (max res)	2.6%
Multiplicity (all data)	11.0
Multiplicity (max res)	5.0
Data/restraint/parameters	8800/7/284
GooF	1.067
R[I>2.0σ(I)],[a] wR2 [I>2.0σ(I)][a]	0.0569, 0.1828
R (all data),[a] wR2 (all data)[a]	0.0571, 0.1830

[a] $R_1 = \Sigma \, ||Fo|-|Fc|| \, / \, \Sigma|Fo|$, $wR_2 = [\Sigma \, w \, (Fo^2 - Fc^2)^2 \, / \, \Sigma w \, (Fo^2)^2]^{½}$

Table S2. Selected coordination distances (Å) and angles (°) for [Ru([9]aneS_3)Cl(cppH)]Cl ·0.45H_2O (**10**)).

Bond distances (Å)			
Ru1–Cl1	2.4316(7)	Ru1–S21	2.305(1)
Ru1–N31	2.094(3)	Ru1–S22	2.2943(8)
Ru1–N32	2.096(2)	Ru1–S23	2.2787(8)
Bond angles (°)			
N31–Ru1–Cl1	88.57(6)	N32–Ru1–S23	94.65(7)
N31–Ru1–N32	77.9(1)	S21–Ru1–Cl1	88.58(3)
N31–Ru1–S21	174.75(7)	S22–Ru1–Cl1	89.92(3)
N31–Ru1–S22	96.31(7)	S22–Ru1–S21	88.09(3)
N31–Ru1–S23	94.40(7)	S23–Ru1–Cl1	176.78(3)
N32–Ru1–Cl1	87.20(7)	S23–Ru1–S21	88.56(3)
N32–Ru1–S21	97.55(7)	S23–Ru1–S22	88.50(3)
N32–Ru1–S22	173.59(7)		

Table S3. Minimal inhibitory concentrations (MIC, μg/mL) of compounds **1-4, 7, 8** and **11** on Gram-positive and Gram-negative bacterial strains. n.a. = not active

Compound	*E. coli*	*A. baumannii*	*P. aeruginosa*	*B. subtilis*	*S. aureus*	*S. aureus*
1	n.a.	n.a.	n.a.	n.a.	n.a.	n.a.
2	n.a.	n.a.	n.a.	n.a.	n.a.	n.a.
3	n.a.	n.a.	n.a.	n.a.	n.a.	n.a.
4	n.a.	n.a.	n.a.	n.a.	n.a.	n.a.
7	n.a.	n.a.	n.a.	256	n.a.	n.a.
8	512	n.a.	n.a.	n.a.	n.a.	n.a.
11	32	n.a.	n.a.	256	n.a.	n.a.